Monthly Notices
of the
ROYAL ASTRONOMICAL SOCIETY

MNRAS **476,** 4713–4718 (2018)
Advance Access publication 2018 March 6

doi:10.1093/mnras/sty582

The radius of the quiescent neutron star in the globular cluster M13

A. W. Shaw,[1★] C. O. Heinke,[1] A. W. Steiner,[2,3] S. Campana,[4] H. N. Cohn,[5] W. C. G. Ho,[6,7] P. M. Lugger[5] and M. Servillat[8]

[1]*Department of Physics, University of Alberta, CCIS 4-181, Edmonton, AB T6G 2E1, Canada*
[2]*Department of Physics and Astronomy, University of Tennessee, Knoxville, TN 37996, USA*
[3]*Physics Division, Oak Ridge National Laboratory, Oak Ridge, TN 37831, USA*
[4]*INAF - Osservatorio astronomico di Brera, Via E. Bianchi 46, I-23807 Merate (LC), Italy*
[5]*Department of Astronomy, Indiana University, 727 E. Third Street, Bloomington, IN 47405, USA*
[6]*Department of Physics and Astronomy, Haverford College, 370 Lancaster Ave, Haverford, PA 19041, USA*
[7]*Mathematical Sciences, Physics & Astronomy and STAG Research Centre, University of Southampton, Southampton SO17 1BJ, UK*
[8]*LUTH, Observatoire de Paris, PSL Research University, CNRS, Université Paris Diderot, F-92190 Meudon, France*

Accepted 2018 February 28. Received 2018 February 27; in original form 2018 January 31

ABSTRACT

X-ray spectra of quiescent low-mass X-ray binaries containing neutron stars can be fit with atmosphere models to constrain the mass and the radius. Mass-radius constraints can be used to place limits on the equation of state of dense matter. We perform fits to the X-ray spectrum of a quiescent neutron star in the globular cluster M13, utilizing data from *ROSAT*, *Chandra*, and *XMM–Newton*, and constrain the mass–radius relation. Assuming an atmosphere composed of hydrogen and a 1.4 $M_\odot$ neutron star, we find the radius to be $R_{\rm NS} = 12.2^{+1.5}_{-1.1}$ km, a significant improvement in precision over previous measurements. Incorporating an uncertainty on the distance to M13 relaxes the radius constraints slightly and we find $R_{\rm NS} = 12.3^{+1.9}_{-1.7}$ km (for a 1.4$M_\odot$ neutron star with a hydrogen atmosphere), which is still an improvement in precision over previous measurements, some of which do not consider distance uncertainty. We also discuss how the composition of the atmosphere affects the derived radius, finding that a helium atmosphere implies a significantly larger radius.

Key words: stars: neutron – globular clusters: general – globular clusters: individual: M13 – X-rays: binaries.

1 INTRODUCTION

One of the unanswered questions in astrophysics concerns the interior physics of neutron stars (NSs), primarily the equation of state (EOS) of dense matter. The EOS, which also defines the relationship between mass and radius, is universal across all NSs (Lattimer & Prakash 2001). However, constraining this relation is difficult due to the complications involved with measuring NS radii. It is possible to derive constraints on the radius of a NS ($R_{\rm NS}$) from spectral fits to their thermal X-ray emission, for example, through spectroscopic observations of thermonuclear bursts (e.g. Özel, Güver & Psaltis 2009; Özel, Gould & Güver 2012; Poutanen et al. 2014; Özel et al. 2016a; Nättilä et al. 2017). Pulse profile modelling of rotation-powered pulsars can also provide an independent, non-spectroscopic method of constraining $R_{\rm NS}$ (Özel et al. 2016b; Watts et al. 2016). One key method of deriving EOS constraints has been through the fitting of X-ray spectra of quiescent low mass X-ray binaries (qLMXBs) containing NSs.

These systems typically exhibit soft X-ray spectra consisting of a thermal, blackbody-like component, sometimes with a harder, non-thermal component (Campana et al. 1998). The nature of the thermal component has been debated over the last few decades. Brown, Bildsten & Rutledge (1998) claimed that the soft X-ray component can be explained by the 'leakage' of heat deposited in the core during accretion episodes. This 'deep crustal heating' model can predict the thermal spectrum of many qLMXBs (e.g. Rutledge et al. 2001a), though not for those which exhibit short accretion episodes, in which case the heat must be released at a shallower depth (Degenaar, Brown & Wijnands 2011). Some qLMXBs may continue to accrete at a low level, somewhat mimicking the spectrum of deep crustal heating (Zampieri et al. 1995).

Regardless of the mechanism powering the soft component, the X-rays originate from the atmosphere of the NS. After accretion ceases, the elements stratify very quickly, leaving the lightest at the top (Alcock & Illarionov 1980; Romani 1987). Thus, studies of qLMXBs have often found that the soft X-ray spectra can be well described by a hydrogen atmosphere (e.g. Rutledge et al. 2001a,b; Heinke et al. 2006) and can therefore provide valuable constraints on NS masses and radii.

★ E-mail: aarran@ualberta.ca

However, the derived radius constraints are heavily dependent on distance measurements, which are not well known for many LMXBs. Instead, we turn to qLMXBs located in globular clusters, whose distances are known to within ∼5–10 per cent (Brown et al. 1998; Rutledge et al. 2002a). With accurate distance measurements, constraints on the NS EOS have been derived from studies of a number of globular cluster qLMXBs. Of the ∼50 known qLMXBs in globular clusters, a relatively small fraction have sufficient flux, and low enough extinction for dedicated studies of the NS EOS. These include qLMXBs in 47 Tuc (X5 and X7; Heinke et al. 2003, 2006; Bogdanov et al. 2016), M13 (Gendre, Barret & Webb 2003b; Webb & Barret 2007; Catuneanu et al. 2013), ω Cen (Rutledge et al. 2002b; Gendre, Barret & Webb 2003a; Webb & Barret 2007; Heinke et al. 2014), M28 (source 26; Becker et al. 2003; Servillat et al. 2012), NGC 6397 (U24; Grindlay et al. 2001; Guillot, Rutledge & Brown 2011a; Heinke et al. 2014), NGC 6304 (Guillot et al. 2009a,b, 2013), NGC 2808 (Webb & Barret 2007; Servillat et al. 2008), NGC 6553 (Guillot et al. 2011b), and M30 (Lugger et al. 2007; Guillot & Rutledge 2014).

Many previous studies have assumed that the atmosphere of the NS in a qLMXB is purely hydrogen (e.g. Guillot et al. 2013, and references therein). This is a reasonable assumption for typical LMXBs with main-sequence donors, as once accretion stops the accreted elements will stratify (Alcock & Illarionov 1980; Romani 1987). However, it has been noted that between 28 and 44 per cent of observed bright globular cluster LMXBs are ultracompact sources (i.e. they have orbital periods <1 h; see Bahramian et al. 2014), suggesting that they require degenerate white dwarf companions devoid of hydrogen, as main-sequence stars are not compact enough to exist in such a small orbit. If this fraction transfers to the quiescent population, then it is likely that a significant number of qLMXBs in globular clusters contain NSs with atmospheres composed of heavier elements (He, C, O).

If this is the case, then an X-ray spectrum incorrectly modelled with a hydrogen atmosphere will underestimate the radius, as spectral fits with heavier element atmospheres give larger radii than H atmospheres (Ho & Heinke 2009). The atmosphere of the NS therefore has important consequences for the EOS and must be considered (e.g. Servillat et al. 2012; Steiner et al. 2018). Unfortunately, it is difficult to determine the correct atmosphere to use without utilizing optical observations to detect (or not) hydrogen in the optical spectrum of LMXBs (e.g. Haggard et al. 2004; Degenaar et al. 2010) or identifying the orbital period (e.g. Heinke et al. 2003). We note here that low-level accretion can work to prevent the stratification of elements (Rutledge et al. 2002a), which would introduce additional uncertainties in X-ray spectral models. However, the lack of variability in the majority of globular cluster qLMXBs suggests that the accretion is not a dominant process, and therefore the accretion rate is low enough to allow the atmosphere to stratify (Bahramian et al. 2015; Walsh, Cackett & Bernardini 2015).

We focus here on the qLMXB source located in the globular cluster M13, discovered by *ROSAT* (Fox et al. 1996; Verbunt 2001) and further studied by the *XMM–Newton* and *Chandra* X-ray observatories (Gendre et al. 2003b; Webb & Barret 2007; Servillat et al. 2011; Catuneanu et al. 2013). Since its discovery, there have been a number of attempts to constrain $R_{\rm NS}$ through X-ray observations. This has resulted in a wide range of measurements, from a relatively compact NS ($R_{\rm NS} \sim$ 9–10 km; Webb & Barret 2007; Guillot et al. 2013), to a much larger one ($R_{\rm NS} \sim$ 12–15, dependent on the chosen atmosphere; Catuneanu et al. 2013).

In this paper, we utilize a new, deep observation of M13 with *XMM–Newton*, deriving the tightest constraints on $R_{\rm NS}$ for this NS yet. We target M13 as the NS has a sufficiently high flux and low hydrogen absorption column ($N_{\rm H}$) where a modest *XMM–Newton* observation can make the largest impact in reducing uncertainty on $R_{\rm NS}$. We discuss our results in the context of the NS EOS and comment on the nature of the NS atmosphere in this particular qLMXB.

Table 1. X-ray observations of M13.

Mission	Observation ID	Date	Detector	GTI (s)
ROSAT	RP300181N00	1992 Sep	PSPCB	45872
XMM–Newton	0085280301	2002 Jan 28	MOS1+MOS2	35222
			PN	14033
XMM–Newton	0085280801	2002 Jan 30	MOS1+MOS2	30868
			PN	12032
Chandra	7290	2006 Mar 9	ACIS-S	27894
Chandra	5436	2006 Mar 11	ACIS-S	26800
XMM–Newton	0760750101	2016 Feb 2	MOS1+MOS2	96653
			PN	81587

2 OBSERVATIONS AND DATA REDUCTION

In this work, we utilize data from *ROSAT*, *Chandra*, and *XMM–Newton*, focusing in particular on a 2016 ∼100 ks observation of M13 with the European Photon Imaging Counter (EPIC) detectors on board *XMM–Newton*. We also use two *XMM–Newton* observations of the cluster from 2002, a pair of archival *Chandra* observations from 2006 and a 1992 *ROSAT* pointing mode observation (see Table 1).

The reduction of the *ROSAT* data and subsequent extraction of the spectrum is described by Webb & Barret (2007) and Catuneanu et al. (2013). However, we reprocessed the *Chandra* and *XMM–Newton* data using a more recent calibration. The *Chandra* data were reduced using CIAO (*Chandra* Interactive Analysis of Observations) v4.9 and the *Chandra* Calibration Database (CALDB) v4.7.3 (Fruscione et al. 2006). The data were reprocessed with the `chandra_repro` script to apply the latest calibration updates and bad pixel files. We filtered the data in the energy range 0.3–10 keV and found no evidence for background flaring. The spectra were extracted from circles of radius 2 arcsec centred on the qLMXB using the CIAO script `specextract`, which also generated the corresponding response matrices.

The *XMM–Newton* data were processed with the Science Analysis System (SAS) v15.0.0. For all observations, we extracted events from the EPIC pn (Strüder et al. 2001) and MOS (Turner et al. 2001) detectors using `epproc` and `emproc`, respectively. All three *XMM–Newton* observations revealed signs of background flaring and were therefore filtered to remove the data affected by the periods of the strongest flaring activity. We use filters of 1, 2, and 0.25 count s^{-1} (MOS) and 4.5, 5, and 0.4 count s^{-1} (pn), for the 2002 January 28, January 30, and 2016 February 2 observations, respectively.

Circular regions with radii of 9.5 arcsec were used to extract the spectra of the NS qLMXB. This ensured that photons from nearby X-ray sources (X6, X9, and X11; Servillat et al. 2011) were excluded (Fig. 1). Response matrices were generated using `rmfgen` and `arfgen` and the spectra were grouped such that they contained at least 20 counts per bin. To achieve better statistics, the two MOS spectra from each observation were combined using the HEASOFT v6.19 tool `addspec`.

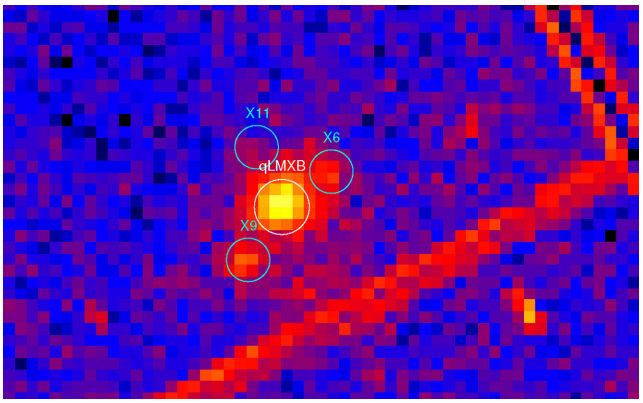

Figure 1. 2016 *XMM–Newton* EPIC pn image of the qLMXB in M13. The white circle represents the region used to extract the source spectrum. The cyan circles highlight the *Chandra* positions of three nearby X-ray sources, X6, X9, and X11 (Servillat et al. 2011).

3 DATA ANALYSIS AND RESULTS

3.1 Spectral fits

All spectral fits were performed using XSPEC v12.9.1p (Arnaud 1996), which uses the χ^2 minimization technique to determine the best fitting model. The interstellar absorption is accounted for by the `tbabs` model with Wilms, Allen & McCray (2000) abundances and photoionization cross-sections described by Verner et al. (1996). In all models, we assume a distance to M13 of $d = 7.7$ kpc (McLaughlin & van der Marel 2005). We choose this distance as it is consistent with (and between) $d = 7.65 \pm 0.36$ kpc as calculated by Sandquist et al. (2010) and $d = 7.8 \pm 0.1$ kpc determined by Recio-Blanco et al. (2005), as well as to be able to draw comparisons with Webb & Barret (2007) and Catuneanu et al. (2013), who both use $d = 7.7$ kpc. We used a normalization constant to account for the cross-calibration differences between each detector, allowing the constant to vary relative to the MOS detectors, for which it was fixed to unity. In all fits, in addition to the relevant NS atmosphere model, we also included a thermal bremsstrahlung model for the fit to the *ROSAT* data, to account for the cataclysmic variable (CV) source X6 (Servillat et al. 2011), which was not resolved as an individual point source by *ROSAT*. We fixed kT of the bremsstrahlung model to 4.5 keV (Webb & Barret 2007; Catuneanu et al. 2013). All uncertainties are quoted at the 90 per cent confidence level, unless otherwise stated.

3.1.1 Hydrogen atmosphere model

We fit the *XMM–Newton*, *Chandra*, and *ROSAT* spectra simultaneously with an absorbed hydrogen atmosphere model `nsatmos` (Heinke et al. 2006). The spectra are plotted in Fig. 2 and the best-fitting model parameters are displayed in Table 2, assuming a fixed NS mass of $M_{\rm NS} = 1.4\,{\rm M}_\odot$. The resulting absorption column is consistent with $N_{\rm H} = (1.74 \pm 0.87) \times 10^{20}$ cm^{-2} in the direction of M13, which is inferred from the extinction, $E(B-V) = 0.02 \pm 0.01$,[1] derived by Harris 1996 (2010 edition), and using Bahramian et al. (2015) to convert between A_V and $N_{\rm H}$. We determine a best-fitting NS radius $R_{\rm NS} = 12.2^{+1.5}_{-1.1}$ km. The determined radius is consistent with that of Catuneanu et al. (2013), $R_{\rm NS} = 11.7^{+1.9}_{-2.2}$ km, with tighter constraints. Allowing the mass to vary gives a best-fitting with $M_{\rm NS} = 1.7\,{\rm M}_\odot$ and $R_{\rm NS} = 11.6$ km. To visualize the derived mass–radius relationship, we calculate the χ^2 contours with the `steppar` command in XSPEC and convert this into a probability distribution $\mathcal{L} \propto \exp(-\chi^2/2)$, shown in Fig. 3 (see e.g. Steiner et al. 2018).

[1] http://physwww.mcmaster.ca/percent7Eharris/mwgc.ref

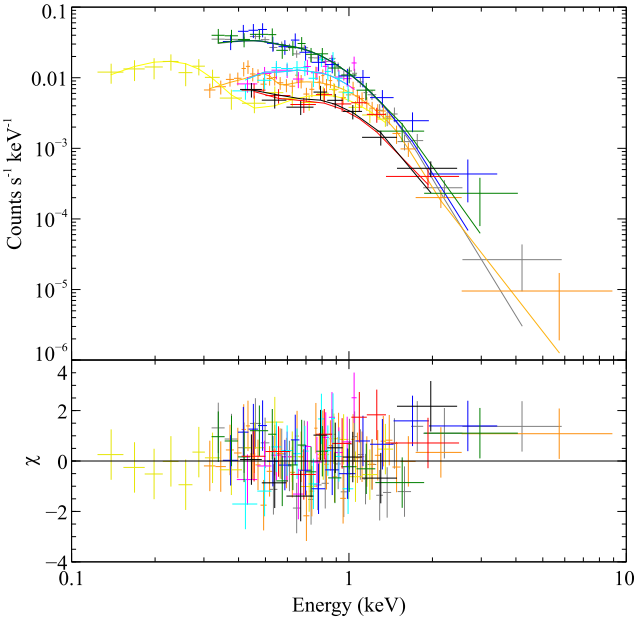

Figure 2. Spectra of the qLMXB in M13, fit with an absorbed hydrogen atmosphere model. Plotted are the 2002 *XMM–Newton* MOS spectra (black and red), 2002 pn spectra (green and blue), 2016 MOS and pn spectra (orange and grey, respectively), 2006 *Chandra* spectra (cyan and magenta), and 1992 *ROSAT* spectrum (yellow). The *ROSAT*data has been fit with an additional bremsstrahlung component to account for the unresolved CV M13 X6. The best-fitting model is plotted as a solid line for each spectrum. The bottom panel shows the $\Delta\chi$ residuals.

Table 2. Best-fitting parameters to the *XMM–Newton*, *Chandra*, and *ROSAT* spectra for hydrogen (`nsatmos`) and helium (`nsx`) atmosphere models, with a NS mass fixed to 1.4 M$_\odot$.

Parameter	`nsatmos`	`nsx`
$N_{\rm H}$	$0.9^{+0.5}_{-0.4} \times 10^{20}$ cm^{-2}	$1.2^{+0.6}_{-0.5} \times 10^{20}$ cm^{-2}
$\log_{10} T_{\rm eff}$	5.97 ± 0.02	$5.92^{+0.02}_{-0.03}$
$R_{\rm NS}$	$12.2^{+1.5}_{-1.1}$ km	$15.1^{+2.0}_{-1.6}$ km
χ^2/dof	128.6/148	123.3/148

3.1.2 Helium atmosphere model

We also fit the spectra with an absorbed helium-atmosphere model `nsx` (Ho & Heinke 2009). The best-fitting model parameters, assuming a 1.4 M$_\odot$ NS, are presented in Table 2. For a 1.4 M$_\odot$ NS, the helium atmosphere model determines a best-fitting NS radius of $15.1^{+2.0}_{-1.6}$ km, ∼3 km larger than that implied by a hydrogen atmosphere. As with the H-atmosphere fits, the inferred absorption column is consistent with that in the direction of M13 (Harris 1996, 2010 edition). If we allow the mass to vary, we find a best-fitting $R_{\rm NS} = 15.1$ km with a $M_{\rm NS} = 1.5\,{\rm M}_\odot$. The mass-radius probability distribution is plotted in Fig. 4.

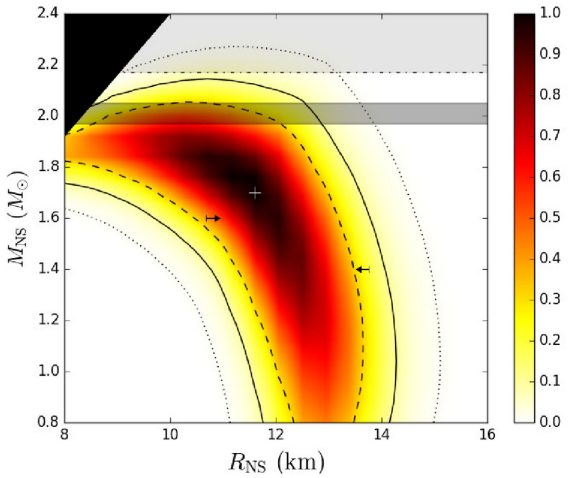

Figure 3. Mass-radius probability distribution for the hydrogen atmosphere model fit to the *XMM–Newton*, *Chandra*, and *ROSAT* spectra of the qLMXB in M13. The dashed, solid, and dotted curves represent the confidence limits at the 68 per cent, 90 per cent, and 99 per cent level, respectively. The black shaded section in the upper left-hand region of the plot represents the area forbidden by causality ($R_{\rm NS} < 2.82GM/c^2$; Haensel, Lasota & Zdunik 1999). The light grey shaded region $M_{\rm NS} > 2.17\,{\rm M}_\odot$ may be disfavoured based on the interpretation of the NS–NS merger GW170817 (e.g. Margalit & Metzger 2017). The narrow, dark grey strip represents the most massive NS measured, PSR J0348+0432 ($M_{\rm NS} = 2.01 \pm 0.04\,{\rm M}_\odot$; Antoniadis et al. 2013). The arrows represent mass-dependent limits on $R_{\rm NS}$ derived from GW170817 (Bauswein et al. 2017; Fattoyev, Piekarewicz & Horowitz 2017).

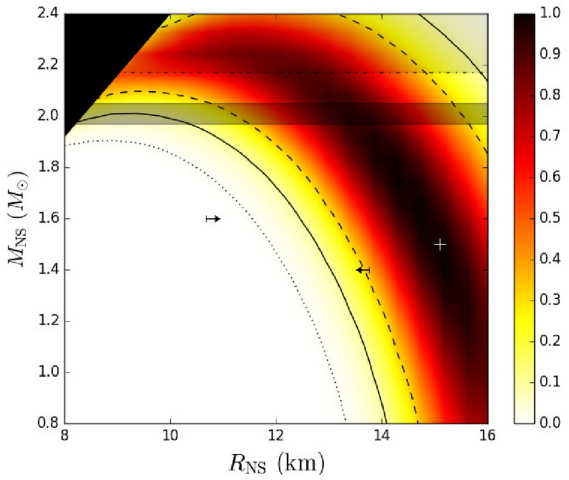

Figure 4. Mass-radius probability distribution for the helium atmosphere model fit to the *XMM–Newton*, *Chandra*, and *ROSAT*spectra of the qLMXB in M13. The key is the same as in Fig. 3.

The helium atmosphere model provides a slightly better fit to the spectra ($\Delta\chi^2 = 5.3$ for the same degrees of freedom) than the hydrogen model. However, both models are considered an acceptable fit to the data. Therefore, it is not possible to determine from the fitting which atmosphere model is the correct one.

4 DISCUSSION

4.1 The effect of distance uncertainty

We have computed our spectral fits assuming a distance to M13 $d = 7.7$ kpc (McLaughlin & van der Marel 2005). However, this did not include its associated uncertainty, which can have an effect on the inferred mass–radius relation. We can incorporate this into the probability distribution by integrating over the distance uncertainty (following the method of Steiner et al. 2018). Using a conservative uncertainty of $\Delta d = \pm 0.36$ kpc (Sandquist et al. 2010), we find $R_{\rm NS} = 12.3^{+1.9}_{-1.7}$ km and $R_{\rm NS} = 15.3^{+2.4}_{-2.2}$ km for a $1.4\,{\rm M}_\odot$ NS with a H and He atmosphere, respectively. As expected, introducing an uncertainty on distance increases the radius uncertainties accordingly. The density distributions are plotted in Fig. 5, and show a similar increase in the mass-radius contours.

4.2 Hydrogen versus helium atmosphere

We have shown that the NS mass and radius constraints are highly dependent on the chosen atmosphere model. If we fix $M_{\rm NS} = 1.4\,{\rm M}_\odot$, we find that $R_{\rm NS}$ increases by $\sim$3 km if the atmosphere is composed of helium versus hydrogen. It is therefore important to distinguish the nature of the companion in order to choose the correct model. Steiner et al. (2018) model the spectra of eight qLMXBs in globular clusters, and combine them to place constraints on the EOS, based on the knowledge that all NSs must have the same EOS (Lattimer & Prakash 2001). Steiner et al. (2018) calculate the probability of the qLMXB in M13 having a helium atmosphere to be < 28 per cent, but with the tighter constraints provided by this work, this probability is likely to be even lower, despite the lower χ^2 for a helium atmosphere model (compared to hydrogen) suggesting a better fit. However, the only reliable way to distinguish between hydrogen and helium atmospheres in NS LMXBs is through direct optical/NIR observations of the counterpart.

4.3 Neutron star equation of state

Our results tighten the constraints on the mass and radius of the NS presented by Catuneanu et al. (2013), which has implications for the NS EOS. Previous studies of M13 claim tighter constraints on $M_{\rm NS}$ and $R_{\rm NS}$ (Gendre et al. 2003b; Webb & Barret 2007) than this work, but these results were not reproduced in later studies (Catuneanu et al. 2013; Guillot et al. 2013). Our results are consistent with Catuneanu et al. (2013) and our derived radius (for a $1.4\,{\rm M}_\odot$ NS) falls within the preferred range of 10–14 km for NSs, calculated from observations of multiple qLMXBs and taking into account the effects that a number of uncertainties (e.g. distance, atmosphere composition) have on the inferred mass–radius relation (Steiner et al. 2018).

A previous study fitting spectra of M13 and other qLMXBs by Guillot et al. (2013) preferred a smaller $R_{\rm NS} = 9.2^{+1.7}_{-2.3p}$ km (where p indicates that the parameter was pegged at the hard limit of the model) for M13. However, in that study, a smaller distance was chosen ($d = 6.5$ kpc; Rees 1996) rather than the 7.7 kpc we utilize in this work (McLaughlin & van der Marel 2005), a distance in agreement with measurements by Recio-Blanco et al. (2005) and Sandquist et al. (2010) (see also Steiner et al. 2018). We note that if we instead choose $d = 6.5$ kpc, we find $R_{\rm NS} = 10.1 \pm 1.4$km, consistent with the value derived by Guillot et al. (2013).

The detection of gravitational waves (GW170817) from two merging NSs (Abbott et al. 2017a) has placed some limits on the NS EOS. The event placed an upper limit on the tidal deformability parameter (Λ, an intrinsic NS property sensitive to the stellar compactness). Limits on the tidal deformability obtained as the two bodies approached coalescence ($\Lambda \leq 800$ for $M_{\rm NS} = 1.4\,{\rm M}_\odot$; Abbott et al. 2017a) can be translated into an upper limit on the radius of a $1.4\,{\rm M}_\odot$ NS ($R_{\rm NS} < 13.76$ km; Fattoyev et al.

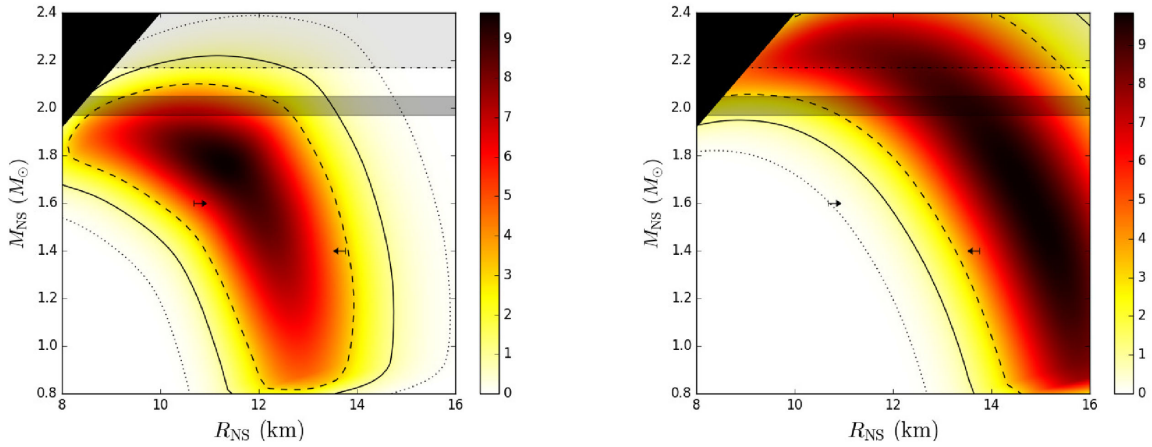

Figure 5. Mass-radius probability distribution (arbitrary normalization) for the hydrogen (left-hand panel) and helium (right-hand panel) model atmosphere fits to the *XMM–Newton*, *Chandra*, and *ROSAT* spectra of the M13 qLMXB, incorporating an uncertainty in the distance of $\delta d = \pm 0.36$ kpc. The key is the same as in Fig. 3.

2017). Information from the short gamma-ray burst that followed the merger 1.7 s later (e.g. Abbott et al. 2017b; Goldstein et al. 2017; Savchenko et al. 2017) can be used to infer a limit on the maximum mass of a NS of $\lesssim 2.17\,{\rm M}_\odot$ (Margalit & Metzger 2017; Shibata et al. 2017; Rezzolla, Most & Weih 2018). We must note, however, that these calculations, though all consistent and performed independently of one another, are heavily dependent on physical assumptions about the type of compact object formed in the merger. Finally, Bauswein et al. (2017) calculated a lower limit of $R_{\rm NS} > 10.68$ km (for $M_{\rm NS} = 1.6\,{\rm M}_\odot$), also assuming that the merger did not result in a prompt collapse to a black hole – as suggested by the detection of a kilonova (Kasen et al. 2017; Pian et al. 2017; Smartt et al. 2017). Though the radius constraints inferred from GW170817 do not fully rule out the possibility of a He atmosphere in the M13 qLMXB, they are in agreement with Steiner et al. (2018) in that it is unlikely to be the case.

5 CONCLUSIONS

We have derived NS mass-radius constraints for the qLMXB located in the globular cluster M13 using archival observations and a new, deep observation of the cluster with *XMM–Newton*. We provide the tightest constraints on the radius of the NS ($R_{\rm NS} = 12.2^{+1.5}_{-1.1}$ km assuming a H atmosphere and $M_{\rm NS} = 1.4\,{\rm M}_\odot$), which are in good agreement with the limits on the NS EOS derived by Steiner et al. (2018). We find that introducing a conservative uncertainty on distance (Sandquist et al. 2010), increases the radius uncertainties accordingly. We cannot definitively rule out a He atmosphere, but spectral fits infer a much larger $R_{\rm NS} = 15.1^{+2.0}_{-1.6}$ km, which overlaps with the upper edge of the $R_{\rm NS} = 10$–14 km range derived by Steiner et al. (2018). In addition, limits on $R_{\rm NS}$ derived from the NS–NS merger GW170817 (Abbott et al. 2017a; Fattoyev et al. 2017) disfavour a He atmosphere interpretation for the qLMXB in M13. To verify the nature of the atmosphere of the NS, we require spectroscopy of the optical/NIR counterpart, which has not yet been discovered.

ACKNOWLEDGEMENTS

We thank the anonymous referee for useful comments which helped improve the manuscript. AWS would like to thank S. Morsink, G. Sivakoff and R. Fernández for useful discussions regarding the NS EOS. COH is supported by an NSERC Discovery Grant and a Discovery Accelerator Supplement. AWS is supported by grant NSF PHY 1554876. WCGH acknowledges funding from STFC in the UK through grant number ST/M000931/1.

REFERENCES

Abbott B. P. et al., 2017a, Phys. Rev. Lett., 119, 161101
Abbott B. P. et al., 2017b, ApJ, 848, L12
Alcock C., Illarionov A., 1980, ApJ, 235, 534
Antoniadis J. et al., 2013, Science, 340, 448
Arnaud K. A., 1996, in Jacoby G. H., Barnes J., eds, ASP. Conf. Ser. Vol. 101, Astronomical Data Analysis Software and Systems V. Astron. Soc. Pac., San Francisco, p. 17
Bahramian A. et al., 2014, ApJ, 780, 127
Bahramian A., Heinke C. O., Degenaar N., Chomiuk L., Wijnands R., Strader J., Ho W. C. G., Pooley D., 2015, MNRAS, 452, 3475
Bauswein A., Just O., Janka H.-T., Stergioulas N., 2017, ApJ, 850, L34
Becker W. et al., 2003, ApJ, 594, 798
Bogdanov S., Heinke C. O., Özel F., Güver T., 2016, ApJ, 831, 184
Brown E. F., Bildsten L., Rutledge R. E., 1998, ApJ, 504, L95
Campana S., Colpi M., Mereghetti S., Stella L., Tavani M., 1998, A&AR, 8, 279
Catuneanu A., Heinke C. O., Sivakoff G. R., Ho W. C. G., Servillat M., 2013, ApJ, 764, 145
Degenaar N. et al., 2010, MNRAS, 404, 1591
Degenaar N., Brown E. F., Wijnands R., 2011, MNRAS, 418, L152
Fattoyev F. J., Piekarewicz J., Horowitz C. J., 2017, preprint (arXiv:1711.06615)
Fox D., Lewin W., Margon B., van Paradijs J., Verbunt F., 1996, MNRAS, 282, 1027
Fruscione A. et al., 2006, inSilva D. R., Doxsey R. E., eds, Proc. SPIE Conf. Ser. Vol. 6270, CIAO: Chandra's data analysis system. SPIE, Bellingham, p. 62701V
Gendre B., Barret D., Webb N. A., 2003a, A&A, 400, 521
Gendre B., Barret D., Webb N., 2003b, A&A, 403, L11
Goldstein A. et al., 2017, ApJ, 848, L14
Grindlay J. E., Heinke C. O., Edmonds P. D., Murray S. S., Cool A. M., 2001, ApJ, 563, L53
Guillot S., Rutledge R. E., 2014, ApJ, 796, L3
Guillot S., Rutledge R. E., Bildsten L., Brown E. F., Pavlov G. G., Zavlin V. E., 2009a, MNRAS, 392, 665

Guillot S., Rutledge R. E., Brown E. F., Pavlov G. G., Zavlin V. E., 2009b, ApJ, 699, 1418
Guillot S., Rutledge R. E., Brown E. F., 2011a, ApJ, 732, 88
Guillot S., Rutledge R. E., Brown E. F., Pavlov G. G., Zavlin V. E., 2011b, ApJ, 738, 129
Guillot S., Servillat M., Webb N. A., Rutledge R. E., 2013, ApJ, 772, 7
Haensel P., Lasota J. P., Zdunik J. L., 1999, A&A, 344, 151
Haggard D., Cool A. M., Anderson J., Edmonds P. D., Callanan P. J., Heinke C. O., Grindlay J. E., Bailyn C. D., 2004, ApJ, 613, 512
Harris W. E., 1996, AJ, 112, 1487
Heinke C. O., Grindlay J. E., Lloyd D. A., Edmonds P. D., 2003, ApJ, 588, 452
Heinke C. O., Rybicki G. B., Narayan R., Grindlay J. E., 2006, ApJ, 644, 1090
Heinke C. O. et al., 2014, MNRAS, 444, 443
Ho W. C. G., Heinke C. O., 2009, Nature, 462, 71
Kasen D., Metzger B., Barnes J., Quataert E., Ramirez-Ruiz E., 2017, Nature, 551, 80
Lattimer J. M., Prakash M., 2001, ApJ, 550, 426
Lugger P. M., Cohn H. N., Heinke C. O., Grindlay J. E., Edmonds P. D., 2007, ApJ, 657, 286
Margalit B., Metzger B. D., 2017, ApJ, 850, L19
McLaughlin D. E., van der Marel R. P., 2005, ApJS, 161, 304
Nättilä J., Miller M. C., Steiner A. W., Kajava J. J. E., Suleimanov V. F., Poutanen J., 2017, A&A, 608, A31
Özel F., Güver T., Psaltis D., 2009, ApJ, 693, 1775
Özel F., Gould A., Güver T., 2012, ApJ, 748, 5
Özel F., Psaltis D., Güver T., Baym G., Heinke C., Guillot S., 2016a, ApJ, 820, 28
Özel F., Psaltis D., Arzoumanian Z., Morsink S., Bauböck M., 2016b, ApJ, 832, 92
Pian E. et al., 2017, Nature, 551, 67
Poutanen J., Nättilä J., Kajava J. J. E., Latvala O.-M., Galloway D. K., Kuulkers E., Suleimanov V. F., 2014, MNRAS, 442, 3777
Recio-Blanco A. et al., 2005, A&A, 432, 851
Rees Jr. R. F., 1996, in Morrison H. L., Sarajedini A., eds, ASP Conf Ser. Vol. 92, Formation of the Galactic Halo...Inside and Out. Astron. Soc. Pac., San Francisco, p. 289
Rezzolla L., Most E. R., Weih L. R., 2018, ApJ, 852, L25
Romani R. W., 1987, ApJ, 313, 718
Rutledge R. E., Bildsten L., Brown E. F., Pavlov G. G., Zavlin V. E., 2001a, ApJ, 551, 921
Rutledge R. E., Bildsten L., Brown E. F., Pavlov G. G., Zavlin V. E., 2001b, ApJ, 559, 1054
Rutledge R. E., Bildsten L., Brown E. F., Pavlov G. G., Zavlin V. E., 2002a, ApJ, 577, 346
Rutledge R. E., Bildsten L., Brown E. F., Pavlov G. G., Zavlin V. E., 2002b, ApJ, 578, 405
Sandquist E. L., Gordon M., Levine D., Bolte M., 2010, AJ, 139, 2374
Savchenko V. et al., 2017, ApJ, 848, L15
Servillat M. et al., 2008, A&A, 490, 641
Servillat M., Webb N. A., Lewis F., Knigge C., van den Berg M., Dieball A., Grindlay J., 2011, ApJ, 733, 106
Servillat M., Heinke C. O., Ho W. C. G., Grindlay J. E., Hong J., van den Berg M., Bogdanov S., 2012, MNRAS, 423, 1556
Shibata M., Fujibayashi S., Hotokezaka K., Kiuchi K., Kyutoku K., Sekiguchi Y., Tanaka M., 2017, Phys. Rev. D, 96, 123012
Smartt S. J. et al., 2017, Nature, 551, 75
Steiner A. W., Heinke C. O., Bogdanov S., Li C., Ho W. C. G., Bahramian A., Han S., 2018, MNRAS,
Strüder L. et al., 2001, A&A, 365, L18
Turner M. J. L. et al., 2001, A&A, 365, L27
Verbunt F., 2001, A&A, 368, 137
Verner D. A., Ferland G. J., Korista K. T., Yakovlev D. G., 1996, ApJ, 465, 487
Walsh A. R., Cackett E. M., Bernardini F., 2015, MNRAS, 449, 1238
Watts A. L. et al., 2016, Rev. Mod. Phys., 88, 021001
Webb N. A., Barret D., 2007, ApJ, 671, 727
Wilms J., Allen A., McCray R., 2000, ApJ, 542, 914
Zampieri L., Turolla R., Zane S., Treves A., 1995, ApJ, 439, 849

This paper has been typeset from a TEX/LATEX file prepared by the author.